Carbon addition effects on microstructure and small-scale hardness for Ti(C,N)-FeNi cermets

H. Besharatloo, M. de Nicolás, J.M. Wheeler, A. Mateo, B. Ferrari, E. Gordo, L. Llanes, J.J. Roa

PII: S0263-4368(19)30531-1
DOI: https://doi.org/10.1016/j.ijrmhm.2019.105064
Article Number: 105064
Reference: RMHM 105064

To appear in: *International Journal of Refractory Metals and Hard Materials*

Received date: 4 July 2019
Revised date: 12 August 2019
Accepted date: 19 August 2019

Please cite this article as: H. Besharatloo, M. de Nicolás, J.M. Wheeler, et al., Carbon addition effects on microstructure and small-scale hardness for Ti(C,N)-FeNi cermets, International Journal of Refractory Metals and Hard Materials, https://doi.org/10.1016/j.ijrmhm.2019.105064

Carbon addition effects on microstructure and small-scale hardness for Ti(C,N)-FeNi cermets.

H. Besharatloo[1,2,*], M. de Nicolás[3], J. M. Wheeler[4], A. Mateo[1,2], B. Ferrari[5], E. Gordo[3], L. Llanes[1,2] and J.J. Roa[1,2]

[1] CIEFMA - Department of Materials Science and Metallurgical Engineering, EEBE, Universitat Politècnica de Catalunya-BarcelonaTech, 08019 Barcelona, Spain

[2] Barcelona Research Centre in Multiscale Science and Engineering, Universitat Politècnica de Catalunya-BarcelonaTech, 08019 Barcelona, Spain

[3] GTP - Department of Materials Science and Engineering, Universidad Carlos III Madrid, Avda. De la Universidad, 30, 28911 Leganés, Spain.

[4] ETH Zürich, Laboratory for Mechanics of Materials and Nanostructures, Department of Materials, Vladimir-Prelog-Weg 5, 8093 Zürich, Switzerland

[5] Institute of Ceramic and Glass, CSIC, 28049 Madrid, Spain

*Corresponding author, e-mail: hossein.besharatloo@upc.edu

Abstract

The current study investigates the influence of carbon addition on the microstructural and micromechanical properties of Ti(C,N)-FeNi cermets with different ceramic/metal phase ratios. Evaluation of small-scale hardness is conducted by using high speed nanoindentation in conjunction with statistical analysis. It allows to gather extremely large data sets (40,000 imprints per grade and condition); and thus, detailed hardness mapping at the microstructure length scale. Subsequent statistical analysis was done by considering three mechanically distinct phases: Ti(C,N) particles, the metallic binder, and one exhibiting the composite behaviour (i.e. imprints probing two-phase regions). In general, it is found that porosity amount is reduced as ceramic/metal phase ratio decreases and carbon is added. Carbon addition is also observed to rise small-scale hardness, but only for two of the defined phases: metallic binder and the composite one. Similar trends are observed regarding the influence of ceramic/metal phase ratio and carbon addition on the inverse hardness-fracture toughness correlation measured under high applied loads.

Keywords: Cermet; High speed indentation; Hardness; Mechanical mapping; Massive indentation; Statistical analysis

1. Introduction

Substitution of traditional WC-Co hardmetals have become a tough challenge for academic and industrial sectors. Main reasons behind it are related to health (toxicity), economic (fluctuating price) and strategic (critical raw materials) considerations [1–3]. In this regard, Ti(C,N)-based cermets have emerged as a competitive alternative system due to their exceptional combination of physical and mechanical properties [4,5]. Regarding the metallic binder, iron (Fe) alloys have been considered as natural substitutes for Co, because their lower price and non-toxicity. Furthermore, Fe is an abundant raw material and has the ability to be hardened by heat treatments [1,6,7]. On the other hand, for an Fe binder phase, nickel (Ni) becomes an optimal alloying element, as previous studies have demonstrated that it improves the wettability between Fe and Ti(C,N). This is essential for achieving full densification of the cermets during the sintering stage [8]. Accordingly, Ti(C,N)-FeNi system have been proposed as a promising competitive alternative for WC-Co for applications where hard materials are required.

The mechanical properties of Ti(C,N)-FeNi cermets at the macroscopic length scale have been reported previously [9,10]. However, little information is available on the micro-scale behaviour of these materials, which is crucial for microstructural design optimization. In this regard, a recent study by the authors have shown that testing protocols based on massive nanoindentation and statistical analysis, previously proposed for characterizing WC-base alloys [11–14], may also be valid for evaluation of small-scale properties of Ti(C,N)-based cermets [15]. Furthermore, such investigation pointed out the effectiveness of FeNi as reinforcement phase for

these materials, towards optimization of hardness-toughness relationships of ceramic-metal systems. In this study, such approach is extended by addressing the influence of carbon addition on microstructure and mechanical properties of Ti(C,N)-FeNi cermets with three different ceramic/metal phase ratios. In doing so, a relatively new high speed nanoindentation mapping technique is employed to analyse and correlate the microstructural and hardness of the constitutive phases at the microstructural length scale. This is achieved by means of massive nanoindentation in conjunction with statistical analysis [16–19].

2. Experimental procedure

2.1. Sample preparation

The main characteristics of the Ti(C,N), Fe and Ni as-received commercial powders used in this investigation are summarized in **Table 1**. The density of the powders was calculated employing a Helium Monosorb Multipycnometer (Quantachrome Corporation, USA). Particle size distribution (average particle size in volume (D_{V50}), Brunauer-Emmett-Taller diameter (D_{BET}) and the agglomeration factor ($F_{ag}= D_{V50}/D_{BET}$) was measured with a laser analyser (Mastersizer S, Malvern instruments Ltd., UK) and the specific surface area (SSA) was characterized by means of one-point nitrogen absorption (Monosorb Surface Area, Quantachrome Corporation, USA).

A combination of powder metallurgy and colloidal processing was used to manufacture the powder compacts, following the procedure described in [9]. Water-suspensions of high solid content of ceramic and metallic powders were separately prepared. The medium pH was modified to 10-11 with tetra-methyl-ammonium hydroxide (TMAH) to stabilize the particle surfaces, and polyethyleneimine (PEI) was added in a 0.4 wt. % to act as dispersant. Ti(C,N) and Fe15Ni slurries were separately milled for 1 h at 50 rpm for homogenization using Si_3N_4 and nylon balls, respectively. For the extra C addition, a 10 g/L graphite suspension was prepared in another vessel, mixing ethanol and Black Carbon (ISTA, Germany), with a mean particle size of 18 μm and density of 2.24 g/cm^3. The ceramic, metallic and graphitic suspensions were blended

according to the formulations collected in **Table 2**. In all of them, the composition of the metal matrix was 85-15 Fe-Ni wt. %. Before spray-drying, a 2 wt. % of polyvinyl alcohol (PVA) was added to the mixture slurries to enable the formation of agglomerates. An Atomizer LabPlant SD-05 (North Yorkshire, UK) was used, with a modified nozzle design to obtain easy-to-press spherical granules, with inlet and exhaust temperatures held constant at 190 and 100 ºC, respectively, a slurry pump rate of 2L/h, and an airflow rate of 29 m^3/h. After atomization, the mixed agglomerates were uniaxially pressed at 600 MPa into 16 mm-diameter disks. The green bodies were sintered in a high-vacuum furnace (10^{-5} mbar) using the following heating cycle: 800 ºC – 30 min, 1450 ºC – 2 h (5 °C/min).

For metallographic and micromechanical characterization, the sintered samples were transversally cut, embedded in conductive resin, and polished with successively smaller diamond pastes down to 3 µm, finishing with a colloidal Al_2O_3 final polish.

2.2. Microstructural characterization

Microstructures of processed and manufactured cermets were analysed using field emission gun scanning electron microscopy (FEG-SEM) to evaluate several parameters of interest: grain size of the Ti(C,N) phase, porosity, and the mean free path of the metallic binder. The carbo-nitride grain size ($d_{Ti(C,N)}$) and mean free path (λ) of the metallic binder were measured by means of the linear interception method (LIM) [20], measured on a minimum of five micrographs per sample. These images were taken using a 7100F FEG-SEM unit (JEOL, Tokyo, Japan) at an acceleration

voltage of 20 kV. In addition, the amount of porosity was determined, by means of ImageJ software, as a function of volume fraction and/or carbon content of the metallic binder.

2.3. Macro-mechanical characterization: Vickers hardness and indentation fracture toughness

Vickers hardness (*HV*) and indentation fracture toughness (K_{Ic}) were evaluated at the macro-metric length scale. *HV* was determined using a diamond Vickers indenter and applied loads 10 and 30 kgf (15 second hold time) using a DuraScan 20 G5 unit (EMCO-TEST Prüfmaschinen GmbH, Kuchl, Austria). K_{Ic} was assessed using Shetty *et al.*'s equation [21], on the basis of length of cracks emanating out of the corner of imprints, resulting after applying a 30kgf load. Residual imprint dimensions and cracks' length were measured using a Phenom XL SEM unit (ThermoFisher Scientific, Waltham, MA, USA).

2.4. Massive nanoindentation and hardness mapping

Hardness cartography maps were obtained by implementing NanoBlitz technique using an iNano® nanoindenter (Nanomechanics Inc., Oak Ridge, USA) with a diamond Berkovich indenter tip. This technique can offer relatively fast testing speeds, wherein positioning of the specimen under the indenter, surface approach, loading, unloading and retracting can be completed in less than 1 s. This novel technique allows *H*- and *E*-mapping over a relatively large

region via indentation grids of thousands of indentations and immediate evaluation following Oliver and Pharr method [22,23]. It provides a large data set that may then be statistically analysed, following the methodology proposed by Ulm and co-workers [16–19], aiming to extract the intrinsic mechanical properties of each constitutive phase, see **Table 2**. In this study, large grids of 40,000 (matrix of 200 by 200) imprints were performed at a maximum load of 10 mN on each sample. The distance between indentations was held constant at 1.5 μm, to prevent significant overlap or effect from neighbouring imprints. It permits to treat each imprint as an independent statistical value. Such spacing value was chosen as it represents 10× the average indentation depth at 10 mN within the majority hard phase, using the spacing criterion suggested by Phani and Oliver [24].

3. Results and discussion

3.1. Microstructural parameters

Secondary electron micrographs for the studied samples are shown in **Figure 1**. Two different phases can be clearly distinguished: Ti(C,N) particles (grey particles) heterogeneously embedded in the FeNi binder (white region). Furthermore, porosity is also discerned as black spots, spread over the samples in both phases. The corresponding microstructural parameters are summarized in **Table 3**.

Porosity was highest in specimens containing 15% Vol. of the metallic binder (**Figure 1** and **Table 3)**. In higher binder content samples, porosity was significantly reduced. Within this context, porosity content may be attributed to insufficient binder to fully wet/enclose all the ceramic particles during the liquid phase sintering. Previous results suggest that the poor sintering of Fe binder cermets reinforced with Ti(C,N) attributes to the low wettability of Fe on TiN. Nevertheless, the addition of small amount of Ni (15 wt. %) to the Fe binder reduces the contact angle of the liquid phase (>90º) to values close to the Ni ones (25º). Consequently, wettability of the binder on TiN is the responsible of the sintering of FeNi binder cermets reinforced with Ti(C,N). Moreover, the calculated phase diagram reveals the evolution of Fe15Ni with respect the carbon content, which demonstrates that an increase in the C content decreases the liquidus temperature. Consequently, the presence of C from the Ti(C,N) substrate is the responsible of the temperature of liquid phase formation, improving the cermet sintering.

In this sense, the addition of C, reduced porosity in all cases and enhanced the hardness [25]. Furthermore, addition of C was observed to reduce porosity in all cases. This C addition effect was more pronounced with increasing binder content - **Figure 2**.

In some samples porosity was observed to exhibit a bimodal distribution, as shown in **Figure 2** for the 30FeNi (sample without carbon). This suggests that large cavities were left unfilled at interfaces or inside agglomerated particles, in addition to small voids inside individual Ti(C,N) particles. It could be rationalized on the basis of incomplete sintering and may be responsible for the relatively large scatter in porosity of these samples. This bimodal distribution of porosity was also seen in the 20FeNi (without carbon addition) - **Figure 3**.

Porosity related to incomplete sintering was observed to disappear with the addition of 0.5 wt. % of carbon (see **Figure 3**). Addition of carbon is known to decrease solidus and liquidus temperatures of the metallic matrix, as well as to increase the temperature range between them. Consequently, a more homogeneous and less porous microstructure is achieved [26–29]. This is confirmed by thermal simulation and differential thermal analysis (DTA) measurements - **Figure 4**. Such phenomenon enhances liquid phase sintering and densification of the material, yielding lower final porosity levels. Moreover, optimization of the carbon addition may improve the wettability of the ceramic phase by the metallic one. Further information on the effect of carbon addition on the microstructural parameters of the studied materials may be found in Refs. [25,30–32].

3.2. Macro hardness assessment

Macro-scale Vickers hardness is one of the standard parameters used for industry for immediate quality control purposes. **Table 4** summarizes the assessed Vickers hardness values performed at different applied loads. **Figure 5** illustrates the influence of both binder content and carbon addition on Vickers hardness (HV10) of investigated cermets. In general, and as expected, Vickers hardness decreases as the binder content increases. Addition of carbon yields similar hardness increase effect. The influence of carbon addition is more evident for samples with higher binder content. Since carbon addition is expected to promote hardening of the metallic binder, its influence is expected to be relatively higher in the grades containing a relatively higher amount of metallic phase. Nevertheless, changes in mechanical properties of the investigated samples should be described as the combined effect of carbon addition on both metallic binder hardening and effective amount of porosity [27,32].

3.3. Indentation fracture toughness

Indentation fracture toughness, or Palmqvist toughness [21], is an established method for evaluating the fracture toughness of cermet materials on the basis of lengths of cracks emanating out of imprint corners, obtained after indentation applying relatively high loads. **Figure 6a** shows a residual imprint of a Vickers indenter together with the induced radial crack system (measuring lines also indicated in **Figure 6a**). **Table 5** and **Figure 6b** demonstrate the influence of binder content and carbon addition on the indentation fracture toughness of investigated

Ti(C,N)-FeNi systems. As expected, it increases dramatically with binder content, highlighting the influence of this variable due to the ductile nature of the metallic phase. The **Figure 6b** also reveals that carbon addition slightly diminishes the indentation fracture toughness, whereas it improves hardness due to the hardening effect in the metallic binder.

3.4. Hardness mapping

Modern high speed nanoindentation techniques allow the performance of large grids of nanoindentations to statistically extract the properties of individual phases and composite behaviour. **Figure 7** illustrates a cropped region of an indentation matrix carried out on the 20FeNi+C sample, in which three kinds of indentation, depending on probing zone, are marked: Ti(C,N) particles (dash-dot circle), metallic binder (solid line circle) and two-phase regions including ceramic/metal interfaces (dashed circle). Since these indentations were performed in load-control mode (load kept constant at 10mN), it can be evidenced that indentations performed on the hard phase are smaller than the ones within the metallic binder. Moreover, some fractures can be observed around Ti(C,N) particles (white arrows), in agreement with brittle response expected for the ceramic phase. Imprints within the metallic binder (solid line circle) show pile-up characteristic of confined plastic deformation, further supporting the intrinsic ductility exhibited by the metallic binder.

Furthermore, **Figure 7** illustrates that spacing between indentations appears sufficient to prevent significant overlap for the majority of impressions, following the criterion of spacing the indentations 10× larger than the indentation depth [24]. There are some exceptions in the softer phase, which were anticipated due to the significant differences in the hardness of the constituent phases. Load chosen for the indentation grid was selected to keep the majority of indentations within the spacing = 10× indent depth criterion, while still maintaining a sufficient depth in the hard phase to yield a representative value.

Hardness maps of three different regions in comparison with corresponding FESEM micrographs are shown in **Figure 8**. Additionally, obtained micrographs and hardness maps were overlaid to offer an illustration of the correlation between the microstructure and micromechanical properties. Several gradient responses, even within individually defined phases, can be distinguished in the hardness maps due to their distinct ranges of colours (**Figure 8**). First, Ti(C,N) particles are tinted with red shades, ranging from 23 up to 30 GPa. Second, metallic binder is manifested in a range from light blue to light green (ranging between 8 up to 15 GPa). Here, higher hardness values are indicative of more constraining (by the surrounding hard phase) of the binder. Third, a composite-like response (defined here as a third mechanically distinct phase) is linked to yellow/orange tones. It describes the interaction of the plastic flow (induced by imprints probing regions including phase boundaries) of both ceramic and metallic constitutive phases. Finally, some dark blue spots can also be observed in direct relation to assessed hardness values below 4 GPa. Such extremely low values are attributed to porosity, as it is sustained by observation of overlaid maps in **Figure 8**.

Figure 9 demonstrates the hardness cartography maps which are attained from 40,000 indentations (matrices of 200x200) performed at 10mN applied load on different samples with carbon addition. Obtained maps manifest the inverse relationship between the evaluated mechanical property and the volume fraction of metallic phase, which attributes to the constraining effect imposed on metallic binder by the harder phase. More information can be found in Ref [15].

3.5. Statistical analysis of hardness cartography maps

Previously, the data extracted from the massive nanoindentation grids was qualitatively compared to the sample morphology. In order to extract the hardness of each individual phase, a statistical analysis (proposed by Ulm and co-workers [16–19]) was performed on the data. **Figure 10** shows a representative histogram of hardness values with a constant bin size of 0.5 GPa gathered from 40,000 indentations performed on the 20FeNi+C sample. As can be seen in **Figure 8**, three discrete peaks were fitted, corresponding to the two constitutive phases and a third composite-like one, where probing regions contain ceramic/metal interfaces. The highest peak, mean value of ~ 27 GPa, relates to Ti(C,N) ceramic phase, while the lowest peak, with a mean value of 12.5 GPa, is attributed to the FeNi metallic binder. The intermediate peak, with a mean value of 19.6 GPa, can be considered as the hardness response of the combined interaction of Ti(C,N) and FeNi binder. A similar histogram analysis was performed on every sample in the study. The mean and standard deviation values of small-scale hardness for each of the three defined phases, in all samples studied, are summarized in **Table 6**.

On the basis of data listed in **Table 6**, several observations may be done. First, hardness values of the ceramic particles are observed to remain constant for all samples, regardless of microstructure, volume fraction of ceramic phase (as reported in Ref [15]), and/or carbon addition. Second, and opposite to previous statement, hardness values assessed for both metallic binder and composite-like phases increase as ceramic/metal phase ratio rises. This can be rationalized by the direct effect of increasing ceramic contribution on load-bearing action on one hand, and the indirect influence linked to higher constraint on the effective deformation of the metallic binder (smaller binder mean free path) on the other one.

Moreover, carbon addition is discerned to enhance local hardness of the binder for samples with given ceramic/metal phase ratio. It will then point out carbon-activated hardening mechanisms in the metallic binder. This scenario can be also extended to the composite phase, where hardness values also increased with carbon addition. However, in this case, besides the referred intrinsic hardening effect for the metallic phase, effective reduction of porosity amount within the cermet should also be recalled for explaining such finding, as it will be now discussed.

Carbon addition effects on the hardness of cermets studied, through effective reduction of porosity amount, can be illustrated in **Figure 11**. It shows lower-hardness regions of histograms for samples which displayed greater porosity. Hardness values less than 4 GPa are assumed to correspond to indentations performed in areas with porosity (dark blue spots in **Figure 8**). In both cases, it is clear that carbon addition reduces the number of indentations which encountered

weak porosity-related areas. A similar trend is also observed with increasing the relative amount of binder within the cermet, in agreement with our previous microstructural observations (**Figure 2**).

4. Conclusions

The influence of carbon addition on the microstructural and micromechanical characteristics of Ti(C,N)-FeNi cermets has been investigated. Based on the obtained data, the following conclusions may be drawn:

- Higher volume fraction of metallic phase as well as carbon addition yield more homogeneous and less porous microstructure for the same ceramic/metal ratio. It results in significant changes in hardness and indentation fracture toughness (following the well-established inverse correlation between both mechanical properties), these being more pronounced in the softer grades.

- The addition of carbon results in higher hardness values at macro- and micro- length scales. Such changes are directly related to an intrinsic (small-scale) hardening effect of the metallic phase as well as to an effective reduction of porosity amount affecting the two-phase composite-like hardness.

- Hardness cartography at the microstructural length scale showed an excellent qualitative correlation between micromechanical characteristics (measured from massive nanoindentation) and microstructural assemblage (as evidenced from FESEM inspection).

- Massive nanoindentation and statistical analysis has proven to be a successful tool for analysing small-scale properties of different constitutive phases. It includes not only assessment of intrinsic hardness values but also evaluation of change in these properties for individual or mechanically distinct phases, as related to specific influence of microstructural/processing variables, e.g. carbon addition or ceramic/metal phase ratio.

Acknowledgements

This investigation was supported by the Spanish Ministerios de Economía y Competitividad MINECO through grant MAT2015-70780-C4-P. J.J. Roa acknowledges the Serra Hunter programme of the Generalitat de Catalunya.

References

[1] B. Gries, L. Prakash, WC hardmetals with Iron based binders, in: P. Rödhammer, L. Sigl, H. Wildner, Proceedings of 17th Plansee Seminar, Reutte, Austria, 2009: p. HM 5/1-HM 5/13.

[2] National Toxicology Program. Department of health and human service, (n.d.). http://ntp.niehs.nih.gov/?objectid=03C9AF75-E1BF-FF40-DBA9EC0928DF8B15, in, USA.

[3] M. Grilli, T. Bellezze, E. Gamsjäger, A. Rinaldi, P. Novak, S. Balos, R. Piticescu, M. Ruello, Solutions for critical raw materials under extreme conditions: a review, Materials (Basel). 10 (2017) 285. https://doi.org/10.3390/ma10030285.

[4] P. Ettmayer, H. Kolaska, W. Lengauer, K. Dreyer, Ti(C,N) Cermets - Metallurgy and Properties, Int. J. Refract. Met. Hard Mater. 13 (n.d.). https://doi.org/10.1016/0263-4368(95)00027-G.

[5] A. Bellosi, R. Calzavarini, M.G. Faga, F. Monteverde, C. Zancolò, G.E. D'Errico, Characterisation and application of titanium carbonitride-based cutting tools, J. Mater. Process. Technol. 143–144 (2003) 527–532. http://dx.doi.org/10.1016/S0924-0136(03)00339-X.

[6] B. Wittmann, W.-D. Schubert, B. Lux, WC grain growth and grain growth inhibition in nickel and iron binder hardmetals, Int. J. Refract. Met. Hard Mater. 20 (2002) 51–60. http://dx.doi.org/10.1016/S0263-4368(01)00070-1.

[7] E. Gordo, B. Gómez, E.M. Ruiz-Navas, J.M. Torralba, Influence of milling parameters on the manufacturing of Fe–TiCN composite powders, J. Mater. Process. Technol. 162–163 (2005) 59–64. http://dx.doi.org/10.1016/j.jmatprotec.2005.02.154.

[8] P. Alvaredo, M.D. Dios, B. Ferrari, E. Gordo, Interface study for the design of alternative matrixes in cermets , EPMA . (2015).

[9] M. Dios, Z. Gonzalez, P. Alvaredo, R. Bermejo, E. Gordo, B. Ferrari, Novel colloidal approach for the microstructural improvement in Ti (C, N)/FeNi cermets, J. Alloys Compd. 724 (2017) 327–338. https://doi.org/10.1016/j.jallcom.2017.07.034.

[10] M. Dios, I. Kraleva, Z. González, P. Alvaredo, B. Ferrari, E. Gordo, R. Bermejo, Mechanical characterization of Ti (C, N)-based cermets fabricated through different colloidal processing routes, J. Alloys Compd. 732 (2018) 806–817. https://doi.org/10.1016/j.jallcom.2017.10.274.

[11] J.J. Roa, E. Jimenez-Pique, C. Verge, J.M. Tarragó, A. Mateo, J. Fair, L. Llanes, Intrinsic hardness of constitutive phases in WC–Co composites: Nanoindentation testing, statistical analysis, WC crystal orientation effects and flow stress for the constrained metallic binder, J. Eur. Ceram. Soc. 35 (2015) 3419–3425. https://doi.org/10.1016/j.jeurceramsoc.2015.04.021.

[12] J.J. Roa, E. Jiménez-Piqué, J.M. Tarragó, D.A. Sandoval, A. Mateo, J. Fair, L. Llanes, Hall-Petch strengthening of the constrained metallic binder in WC–Co cemented carbides: experimental assessment by means of massive nanoindentation and statistical analysis, Mater. Sci. Eng. A. 676 (2016) 487–491. https://doi.org/10.1016/j.msea.2016.09.020.

[13] J.J. Roa, P.S. Phani, W.C. Oliver, L. Llanes, Mapping of mechanical properties at microstructural length scale in WC-Co cemented carbides: Assessment of hardness and elastic modulus by means of high speed massive nanoindentation and statistical analysis, Int. J. Refract. Met. Hard Mater. 75 (2018) 211–217. https://doi.org/10.1016/j.ijrmhm.2018.04.019.

[14] D.A. Sandoval, J.J. Roa, O. Ther, E. Tarrés, L. Llanes, Micromechanical properties of WC-(W, Ti, Ta, Nb) C-Co composites, J. Alloys Compd. 777 (2019) 593–601. https://doi.org/10.1016/j.jallcom.2018.11.001.

[15] H. Besharatloo, M. de Nicolás, J.J. Roa, M. Dios, A. Mateo, B. Ferrari, E. Gordo, L. Llanes, Assessment of mechanical properties at microstructural length scale of Ti(C,N)–FeNi ceramic-metal composites by means of massive nanoindentation and statistical analysis, Ceram. Int. (2019). https://doi.org/10.1016/j.ceramint.2019.06.292.

[16] G. Constantinides, F.-J. Ulm, K. Van Vliet, On the use of nanoindentation for cementitious materials, Mater. Struct. 36 (2003) 191–196. https://doi.org/10.1007/BF02479557.

[17] G. Constantinides, K.S. Ravi Chandran, F.J. Ulm, K.J. Van Vliet, Grid indentation analysis of composite microstructure and mechanics: Principles and validation, Mater. Sci. Eng. A. 430 (2006) 189–202. http://dx.doi.org/10.1016/j.msea.2006.05.125.

[18] G. Constantinides, F.-J. Ulm, The nanogranular nature of C–S–H, J. Mech. Phys. Solids. 55 (2007) 64–90. https://doi.org/10.1016/j.jmps.2006.06.003.

[19] F.-J. Ulm, M. Vandamme, C. Bobko, J. Alberto Ortega, K. Tai, C. Ortiz, Statistical Indentation Techniques for Hydrated Nanocomposites: Concrete, Bone, and Shale, J. Am. Ceram. Soc. 90 (2007) 2677–2692. https://doi.org/10.1111/j.1551-2916.2007.02012.x.

[20] Metallographic Determination of Microstructure. Part 2: Measurement of WC Grain Size, in: ISO 4499-2 2008, Hardmetals, Geneva, 2008.

[21] D.K. Shetty, I.G. Wright, P.N. Mincer, A.H. Clauer, Indentation fracture of WC-Co cermets, J. Mater. Sci. 20 (1985) 1873–1882. https://doi.org/10.1007/BF00555296.

[22] W.C. Oliver, G.M. Pharr, An improved technique for determining hardness and elastic modulus using load and displacement sensing indentation experiments, J. Mater. Res. 7 (1992) 1564–1583. https://doi.org/10.1557/JMR.1992.1564.

[23] W.C. Oliver, G.M. Pharr, Measurement of hardness and elastic modulus by instrumented indentation: Advances in understanding and refinements to methodology, J. Mater. Res. 19 (2004) 3–20. https://doi.org/10.1557/jmr.2004.19.1.3.

[24] P. Sudharshan Phani, W.C. Oliver, A critical assessment of the effect of indentation spacing on the measurement of hardness and modulus using instrumented indentation testing, Mater. Des. 164 (2019) 107563. https://doi.org/10.1016/j.matdes.2018.107563.

[25] P. Alvaredo, M. Dios, B. Ferrari, E. Gordo, Understanding of wetting and solubility behavior of Fe binder on Ti (C, N) cermets, J. Alloys Compd. 770 (2019) 17–25. https://doi.org/10.1016/j.jallcom.2018.07.243.

[26] M. Seo, J. Kim, S. Kang, Effect of carbon content on the microstructure and properties of (Ti0. 7W0. 3) C-Ni cermet, Int. J. Refract. Met. Hard Mater. 29 (2011) 424–428. https://doi.org/10.1016/j.ijrmhm.2011.01.004.

[27] P. Alvaredo, S.A. Tsipas, E. Gordo, Influence of carbon content on the sinterability of an FeCr matrix cermet reinforced with TiCN, Int. J. Refract. Met. Hard Mater. 36 (2013) 283–288. https://doi.org/10.1016/j.ijrmhm.2012.10.007.

[28] Y. Zhao, Y. Zheng, W. Zhou, J. Zhang, Q. Huang, W. Xiong, Effect of carbon addition on the densification behavior, microstructure evolution and mechanical properties of Ti (C, N)-based cermets, Ceram. Int. 42 (2016) 5487–5496. https://doi.org/10.1016/j.ceramint.2015.12.097.

[29] M. Chen, Q. Zhuang, N. Lin, Y. He, Improvement in microstructure and mechanical properties of Ti (C, N)-Fe cermets with the carbon additions, J. Alloys Compd. 701 (2017) 408–415. https://doi.org/10.1016/j.jallcom.2017.01.119.

[30] P. Alvaredo, C. Abajo, S.A. Tsipas, E. Gordo, Influence of heat treatment on the high temperature oxidation mechanisms of an Fe–TiCN cermet, J. Alloys Compd. 591 (2014) 72–79. https://doi.org/10.1016/j.jallcom.2013.12.009.

[31] E. Chicardi, Y. Torres, M.J. Sayagués, V. Medri, C. Melandri, J.M. Córdoba, F.J. Gotor, Toughening of complete solid solution cermets by graphite addition, Chem. Eng. J. 267 (2015) 297–305. https://doi.org/10.1016/j.cej.2015.01.022.

[32] P. Alvaredo, P. Bruna, D. Crespo, E. Gordo, Influence of carbon content on microstructure and properties of a steel matrix cermet, Int. J. Refract. Met. Hard Mater. 75 (2018) 78–84. https://doi.org/10.1016/j.ijrmhm.2018.04.006.

List of figures

Figure 7. FESEM micrograph of magnified region of indentation array applied at 10 mN applied force on the 20FeNi+C sample

Figure 8. FESEM micrographs and hardness cartography maps of different selected regions of applied matrix of indentations on 20FeNi+C sample are shown in the left and middle columns, respectively. Combined images showing the hardness maps overlaid on the electron micrographs are shown in the right column.

Figure 9. Hardness cartography map obtained from three different matrices of indentations (200x200) performed at 10mN on (a) 15FeNi+C, (b) 20FeNi+C and (c) 30FeNi+C samples.

Figure 10. Hardness histogram determined from 40,000 indentations performed at a maximum applied load of 10 mN on sample 20FeNi+C.

Figure 11. Hardness histograms for studied samples exhibiting relatively high porosity levels, magnified on the regions corresponding to hardness values lower than 4 GPa.

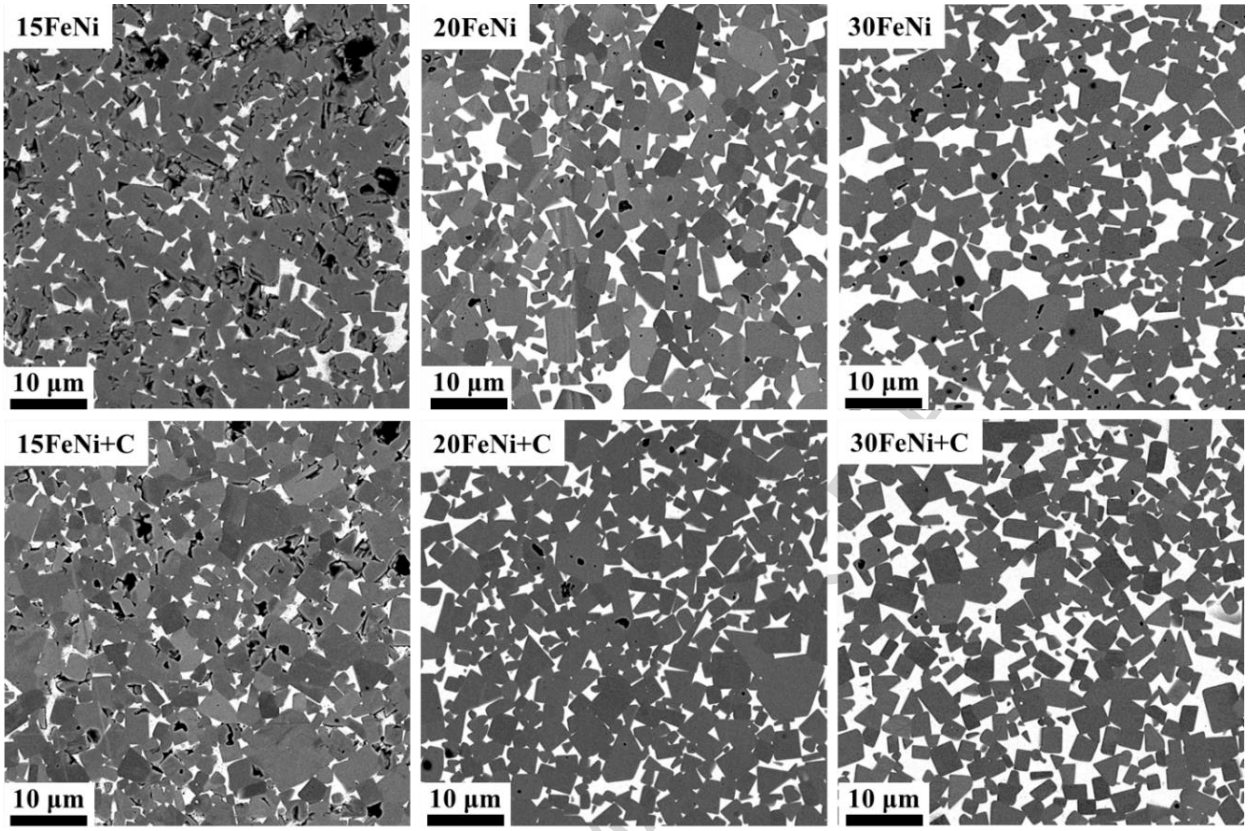

Figure 1. SEM images of Ti(C,N)-FeNi cermets with different vol. % and carbon addition of the metallic binder.

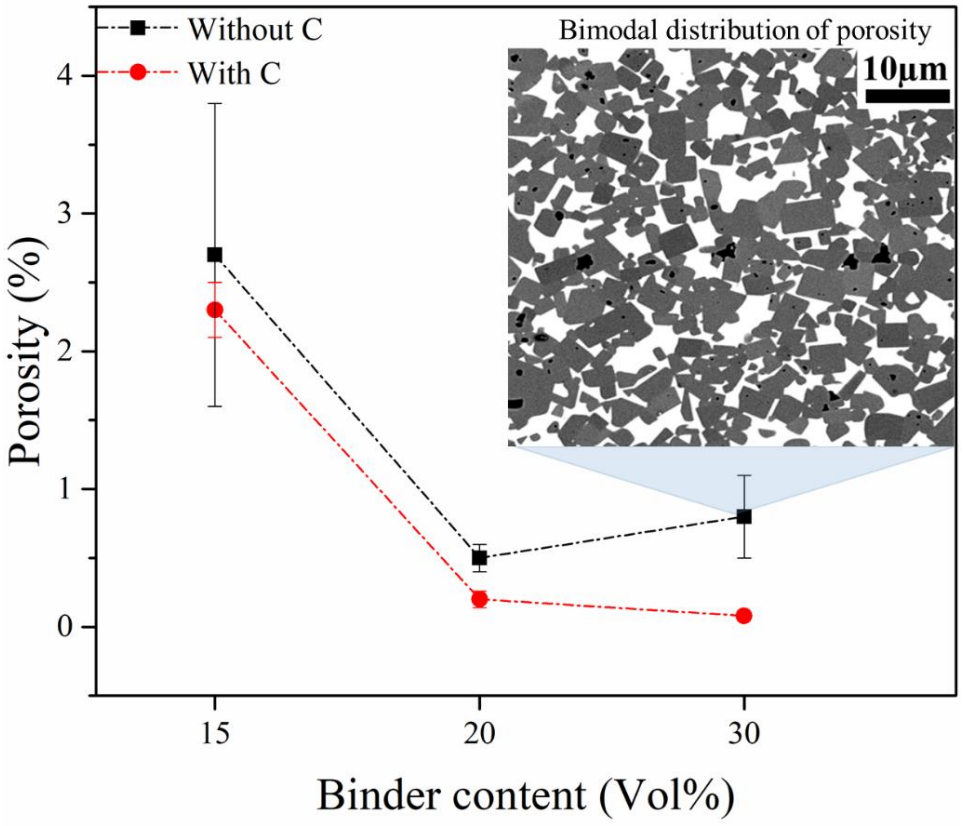

Figure 2. Porosity versus binder content for samples with (red) and without (black) carbon content.

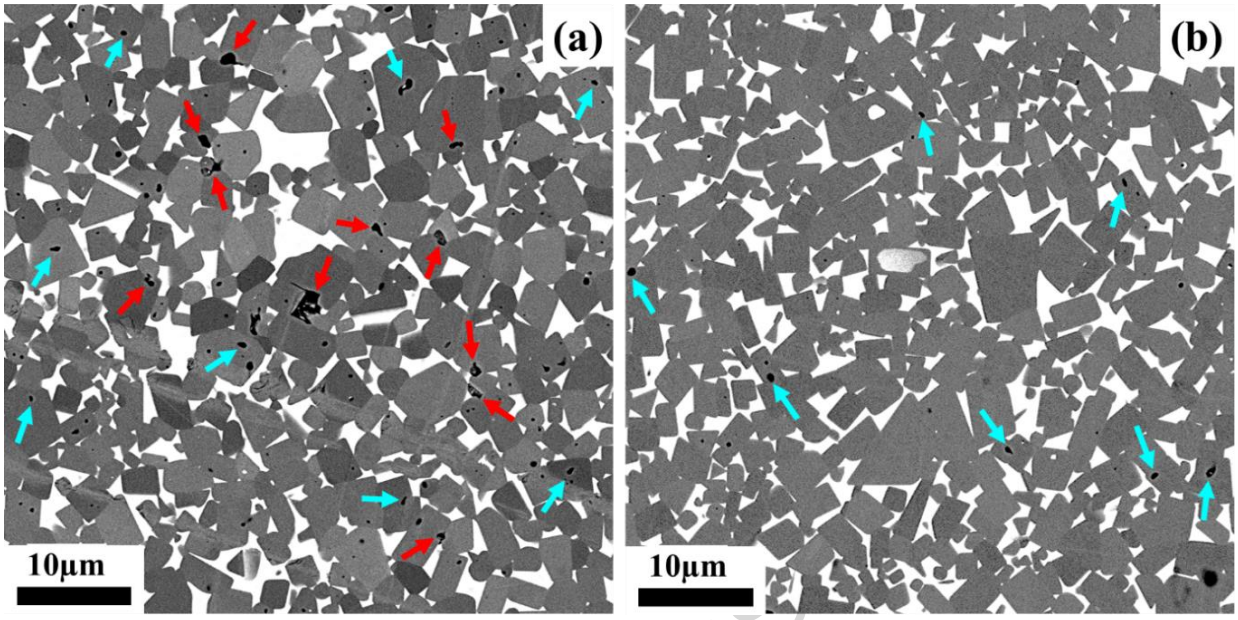

Figure 3. Porosities of the samples with 20 vol. % of the metallic binder, (a) without carbon addition and (b) with carbon addition.

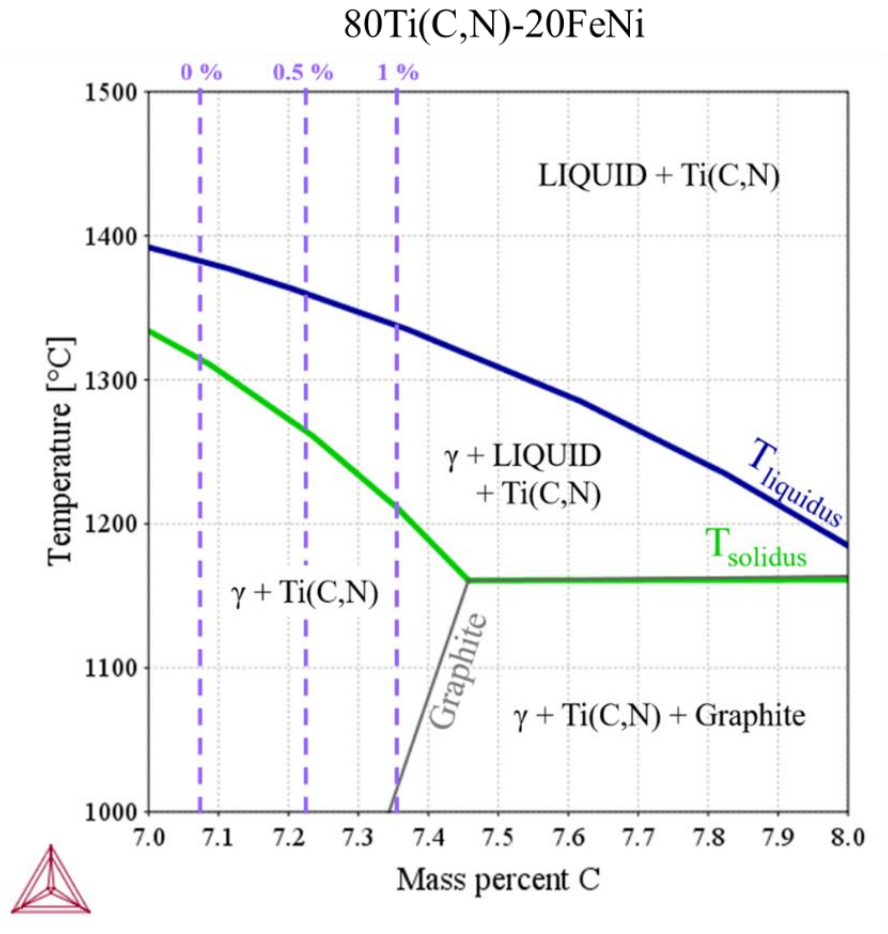

Figure 4. Equilibrium phase diagram (simulated by Thermo-Calc) for sample with 20 Vol.% of the metallic binder.

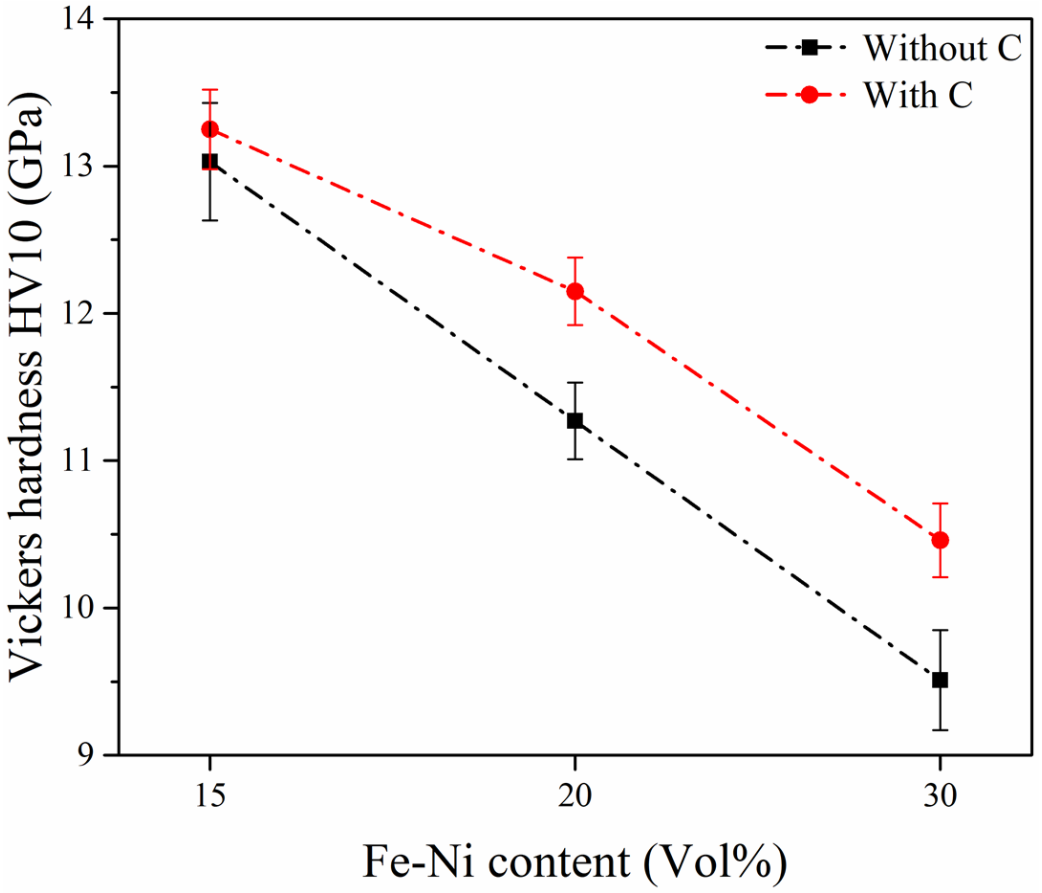

Figure 5. Influence of binder content and carbon (C) addition on HV for all the different samples.

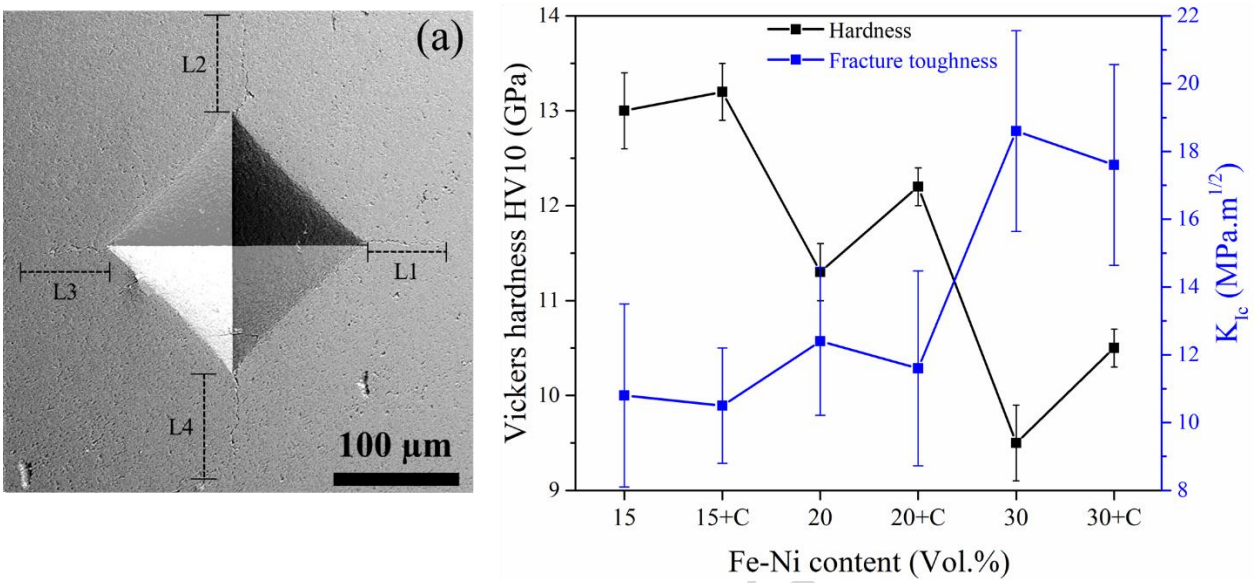

Figure 6. (a) Residual Vickers imprint applied on 20FeNi+C sample at 30 kgf, (b) Influence of binder content and carbon addition on the Vickers hardness and indentation fracture toughness of studied samples.

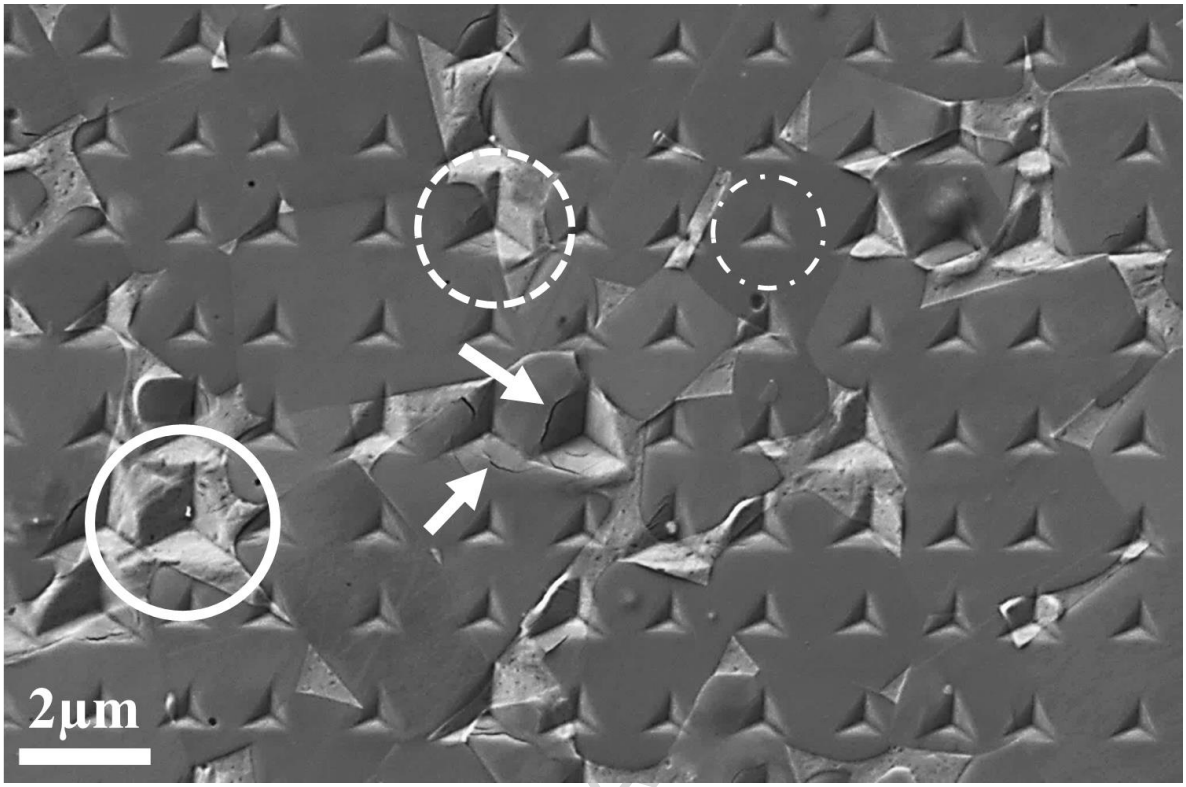

Figure 7. FESEM micrograph of magnified region of indentation array applied at 10 mN applied force on the 20FeNi+C sample

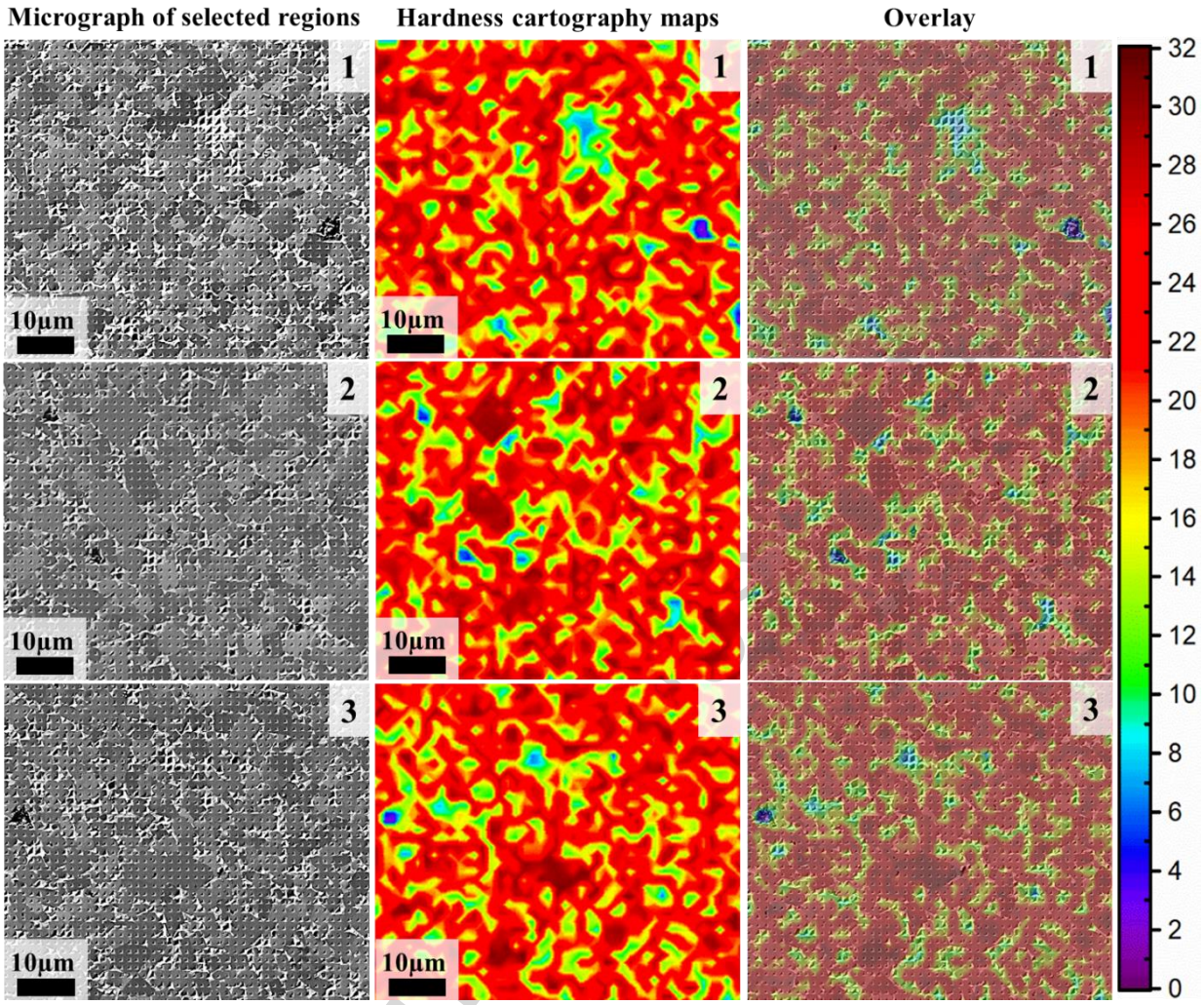

Figure 8. FESEM micrographs and hardness cartography maps of different selected regions of applied matrix of indentations on 20FeNi+C sample are shown in the left and middle columns, respectively. Combined images showing the hardness maps overlaid on the electron micrographs are shown in the right column.

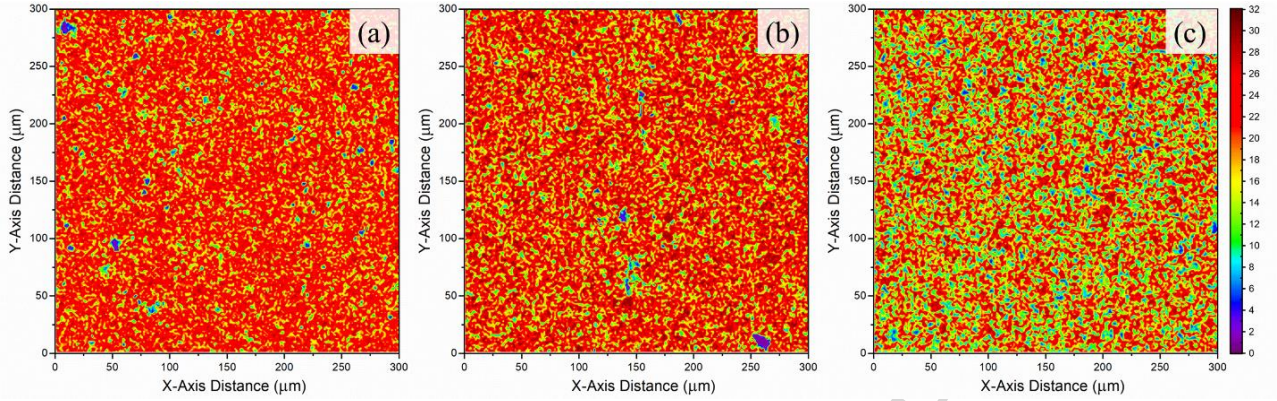

Figure 9. Hardness cartography map obtained from three different matrices of indentations (200x200) performed at 10mN on (a) 15FeNi+C, (b) 20FeNi+C and (c) 30FeNi+C samples.

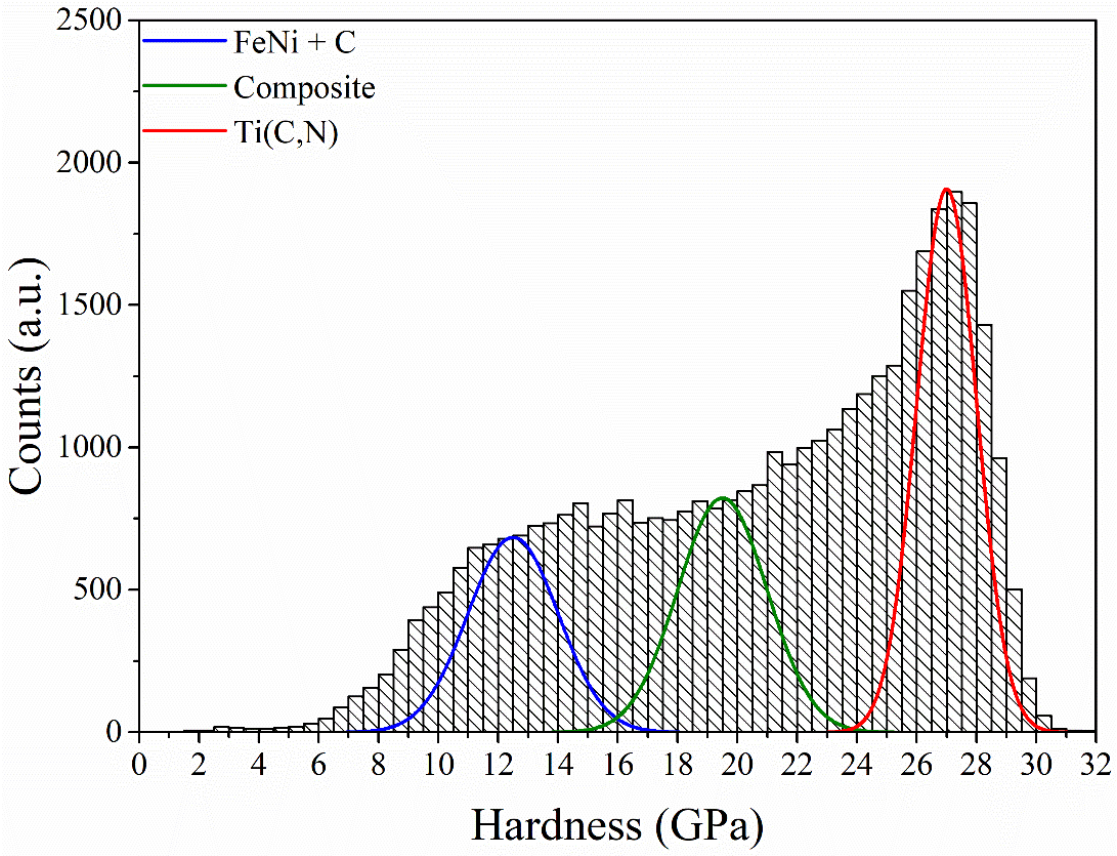

Figure 10. Hardness histogram determined from 40,000 indentations performed at a maximum applied load of 10 mN on sample 20FeNi+C.

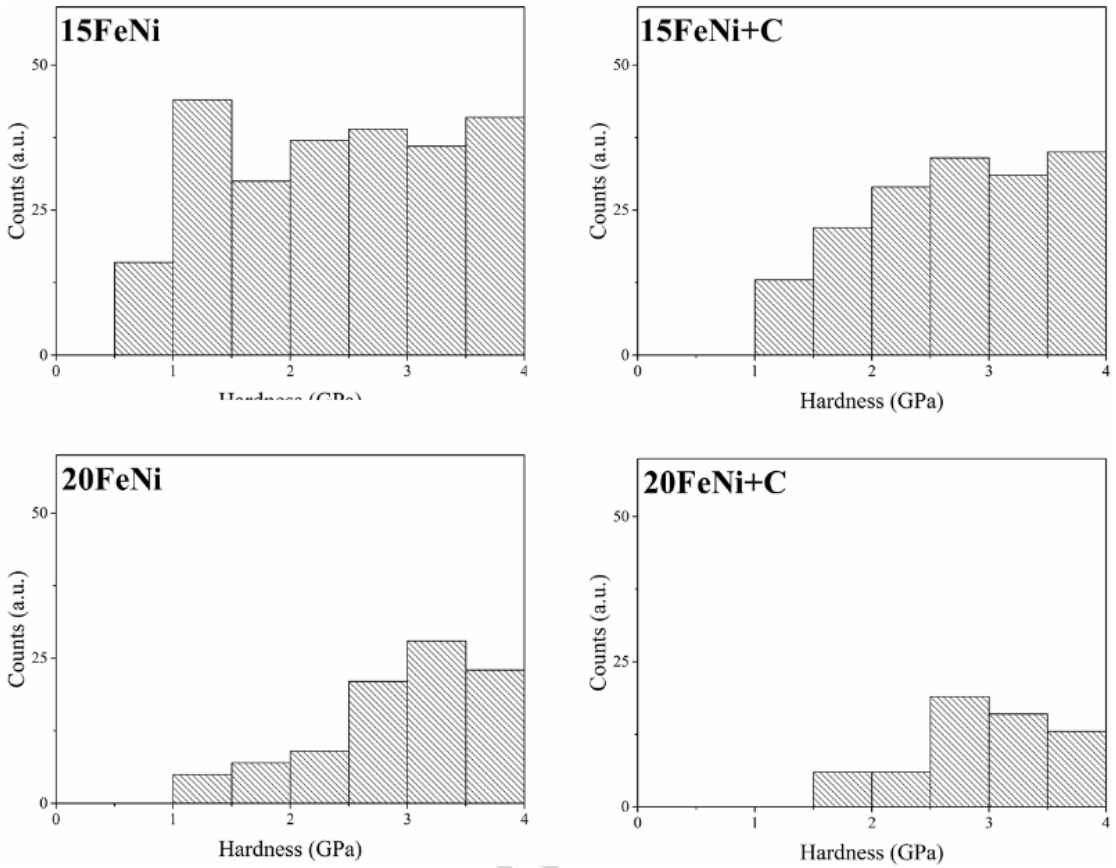

Figure 11. Hardness histograms for studied samples exhibiting relatively high porosity levels, magnified on the regions corresponding to hardness values lower than 4 GPa.

List of tables

Table 1. Main characteristics of the as-received commercial powders.

Powder	Type/Supplier	[a] Density (g/cm^3)	Particle size distribution			[b] SSA (m^2/g)
			D_{V50} (μm)	D_{BET} (μm)	F_{ag} (-)	
Ti(C,N)	$Ti(C_{0.5},N_{0.5})$/H.C.Starck (Germany)	5.1	2.1	0.4	5.0	3.0
Fe	Fe SM/H.C.Starck (Germany)	7.8	3.5	1.2	3.0	0.6
Ni	Ni 210H/INCO (Canada)	8.9	1.7	0.2	10	4.0

[a] ±0.1 Standard deviation in density measurements.

[b] ±0.1 Standard deviation in specific surface area measurements.

Table 2. Formulations of the different materials prepared.

Specimen	Volume (Vol. %)		Weight (wt. %)	
	Ti(C,N)	FeNi	Ti(C,N)	FeNi
15FeNi	85	15	78.2	21.8
20FeNi	80	20	71.7	28.3
30FeNi	70	30	59.7	40.3

Table 3. Summary of the microstructural parameters of studied samples.

Sample name	Binder content %	Carbon content %wt	Mean Ti(C,N) grain size, $d_{Ti(C,N)}$ (μm)	Mean free path, λ (μm)	Porosity %
15FeNi	15	0	2.2 ± 0.3	0.5 ± 0.1	2.7 ± 1.1
15FeNi+C		0.5	2.3 ± 0.2		2.3 ± 0.2
20FeNi	20	0	2.2 ± 0.3	0.6 ± 0.1	0.5 ± 0.1
20FeNi+C		0.5	2.2 ± 0.3		0.2 ± 0.1
30FeNi	30	0	2.3 ± 0.3	1.0 ± 0.2	0.8 ± 0.2
30FeNi+C		0.5	2.3 ± 0.3		0.1 ± 0.1

Table 4. Summary of the HV values obtained at 10 and 30 kgf of maximum applied load.

Sample	HV10 (GPa)	HV 30 (GPa)
15FeNi	13.0 ± 0.4	12.8 ± 0.1
15FeNi + C	13.3 ± 0.3	13 ± 0.1
20FeNi	11.3 ± 0.3	11 ± 0.1
20FeNi + C	12.2 ± 0.2	11.7 ± 0.1
30FeNi	9.5 ± 0.4	9.1 ± 0.2
30FeNi + C	10.5 ± 0.2	9.9 ± 0.2

Table 5. Indentation fracture toughness of studied samples.

Sample	Indentation fracture toughness (MPa·√m)
15FeNi	10.8 ± 2.7
15FeNi + C	10.5 ± 1.7
20FeNi	12.4 ± 2.2
20FeNi + C	11.6 ± 2.9
30FeNi	20.8 ± 2.0
30FeNi + C	17.6 ± 3.0

Table 6. Summary of the hardness mean values for each phase of the investigated samples obtained through the statistical analysis.

Sample	Hardness (GPa)		
	FeNi	Composite	Ti(C,N)
15FeNi	13.7 ± 0.3	20.4 ± 0.2	26.8 ± 0.2
15FeNi+C	14.1 ± 0.3	21.5 ± 0.2	26.9 ± 0.2
20FeNi	11.7 ± 0.2	19.1 ± 0.2	26.7 ± 0.2
20FeNi+C	12.5 ± 0.2	19.6 ± 0.1	26.9 ± 0.2
30FeNi	8.3 ± 0.3	15.0 ± 0.3	26.6 ± 0.3
30FeNi+C	9.6 ± 0.2	17.1 ± 0.2	26.7 ± 0.3

Highlights

- Influence of ceramic/metallic ratio and Carbon addition on mechanical properties of Ti(C,N)-FeNi composite in both macro and micro metric length-scale have been studied.
- Inclusive hardness cartography maps have been executed by means of high speed nanoindentation base mapping technique and checked with associated microstructure of indenting regions.
- Influence of binder volume fraction and carbon addition on microstructure and micromechanical properties of studied cermets were observed by means of indentation mapping for the first time.